Publication Year	2020
Acceptance in OA@INAF	2021-11-30T15:43:25Z
Title	Helium abundance (and H_0) in X-COP galaxy clusters
Authors	ETTORI, STEFANO; Ghirardini, V.; Eckert, D.
DOI	10.1002/asna.202023780
Handle	http://hdl.handle.net/20.500.12386/31193
Journal	ASTRONOMISCHE NACHRICHTEN
Number	341

Received 2019; | Revised 2019; | Accepted 2019
DOI: xxx/xxxx

arXiv:1911.05039v2 [astro-ph.CO] 3 Dec 2019

ORIGINAL PAPER

Helium abundance (and H_0) in X-COP galaxy clusters

S. Ettori*[1,2] | V. Ghirardini[3] | D. Eckert[4]

[1]INAF, Osservatorio di Astrofisica e Scienza dello Spazio, via Pietro Gobetti 93/3, 40129 Bologna, Italy
[2]INFN, Sezione di Bologna, viale Berti Pichat 6/2, I-40127 Bologna, Italy
[3]Center for Astrophysics | Harvard & Smithsonian, 60 Garden Street, Cambridge, MA 02138, USA
[4]Department of Astronomy, University of Geneva, Ch. d'Ecogia 16, CH-1290 Versoix, Switzerland

Correspondence
*Corresponding author; Email: stefano.ettori@inaf.it

We present the constraints on the helium abundance in 12 X-ray luminous galaxy clusters that have been mapped in their X-ray and Sunyaev-Zeldovich (SZ) signals out to R_{200} for the *XMM-Newton* Cluster Outskirts Project (X-COP). The unprecedented precision available for the estimate of H_0 allows us to investigate how much the reconstructed X-ray and SZ signals are consistent with the expected ratio x between helium and proton densities of 0.08–0.1. We find that an H_0 around 70 km s^{-1} Mpc^{-1} is preferred from our measurements, with lower values of H_0 as suggested from the Planck collaboration (67 km s^{-1} Mpc^{-1}) requiring a 34% higher value of x. On the other hand, higher values of H_0, as obtained by measurements in the local universe, impose an x, from the primordial nucleosynthesis calculations and current solar abundances, reduced by 37–44%.

KEYWORDS:
galaxies: clusters: general – X-rays: galaxies: clusters – (galaxies:) intergalactic medium – (cosmology:) cosmological parameters

1 | INTRODUCTION

Galaxy clusters form under the action of gravity by the accretion onto a dark matter halo of primordial gas, mostly composed by hydrogen and helium. During its hierarchical assembly, this intracluster medium (ICM) is heated up to temperatures of $10^7 - 10^8$ K, making it an almost fully ionized plasma, which produces both X-ray emission through bremsstrahlung radiation and line emission, and a characteristic spectral distortion of the cosmic microwave background (CMB) signal due to inverse Compton scattering off the hot ICM electrons of the CMB photons, the so-called Sunyaev-Zel'dovich (SZ) effect (Sunyaev & Zeldovich, 1972) detected at microwave wavelengths.

In the ICM, the helium is fully ionized and not directly observable, and can be different from the primordial amount due to, e.g., release from stars, or sedimentation, mostly in cluster cores under the action of the gravitational force. if the suppression due to the magnetic field is modest, diffusion can occur and He (but not heavier metals like Fe) can drift inwards with typical velocity (e.g. Ettori & Fabian, 2006; Spitzer, 1956) $v_{\rm sed} = A_1 A_2 v_{\rm th}^3 g / (Z_1^2 Z_2^2 n_1 \ln \Lambda) \approx 2$ kpc / Gyr ≈ 2 km/s, where labels '1' and '2' identify the two populations of particles with atomic weight A and atomic number Z, $v_{\rm th} = (2kT/A_1 m_{\rm p})^{1/2}$ is the thermal velocity in a plasma with temperature kT in hydrostatic equilibrium with gravitational acceleration g. However, this effect can be significantly limited by the magnetic topology, plasma instabilities, gas mixing by mergers and turbulence. For instance, $v_{\rm sed}$ is well below the expected level of turbulence present in the ICM of few hundred km/s (see e.g. Hitomi Collaboration et al., 2018a; Sanders & Fabian, 2013), making even more inefficient the process to sediment, even partially, into the cluster core and within the Hubble time. If helium sedimentation occurs, however, the expected impact is very limited: an enhancement by 10% of the helium abundance has been shown to affect only the metal abundances by 0.02–0.03 over the Hitomi SXS band (Hitomi Collaboration et al., 2018b); on the integrated quantities, like gas and total mass, an effect is potentially measurable only in very inner regions, and is negligible when large cluster's volume is considered ($\sim R_{500}$[1]; see e.g. Bulbul et al., 2011).

---

[1] R_{500} indicates the radius of the sphere enclosing an average mass density equal to 500 times the critcal density of the Universe at the cluster's redshift

In the X-ray spectral analysis, it is generally assumed that the helium abundance is equal to its primordial value. At the present, calculations on the Big Bang Nucleosynthesis (BBN) provides rigid predictions on this primordial value, because complementary measurements on, e.g., the number of light neutrino families, the lifetime of the neutron, the baryonic density of the Universe are now constrained at percent level, leaving no more free parameter in standard BBN. Hence, the calculated primordial abundances are in principle only affected by the moderate uncertainties in nuclear cross sections (see e.g. Pitrou, Coc, Uzan, & Vangioni, 2018). These calculations predict $Y_{\rm BBN} = \rho_{\rm He}/\rho_{\rm b} = 0.2471 \pm 0.0002$.

Observational constraints on pristine abundances refer to classes of objects believed to be more primitive, where the metallicity is expected to be less polluted from subsequent enrichment processes by massive stars. For instance, ^{4}He abundance is estimated in HII (ionized hydrogen) regions inside compact blue galaxies, assumed to be the constituents of present-day galaxies in our hierarchical structure formation paradigm. By extrapolating the observed values in these metal poor regions to zero metallicity, $Y = \rho_{\rm He}/\rho_{\rm b}$ is measured to be 0.2449 ± 0.0040 (e.g. Aver, Olive, & Skillman, 2015), well in agreement with $Y_{\rm BBN}$.

The helium abundance affects also the anisotropy in the cosmic microwave background at intermediate angular scales ($1000 \leq l \leq 3000$), the so-called "damping tail" since the anisotropy power on these angular scales is damped by photon diffusion during recombination (Silk, 1968). Planck Collaboration et al. (2018) discusses limits on the estimates of Y, also accounting for the partial degeneration induced from the relativistic degrees of freedom. These constraints are perfectly consistent with $Y_{\rm BBN}$, setting a scenario in which the primordial cosmic helium abundance is known at very high accuracy.

In this context, we investigate with the present study how the estimate of the He abundance affects the observed properties of the ICM, and which constraints we can put on it using the combination of the gas pressure profiles obtained for a well-selected sample of galaxy clusters with independent measurements of their X-ray and SZ signals, and a knowledge on the value of the Hubble constant.

The paper is organized as follows. In the next Section, we describe the method adopted to constrain the He abundance, and the observables used. We present our results in Section 3, drawing some conclusions in Section 4. Unless mentioned otherwise, the quoted errors are statistical uncertainties at the 1σ confidence level, and the cosmological model of reference is a ΛCDM with parameters H_0 =70 km s^{-1} Mpc^{-1} and $\Omega_{\rm m} = 1 - \Omega_\Lambda = 0.3$.

2 | HE ABUNDANCE IN THE ICM

The helium affects the X-ray emission mainly through its contribution to the thermal bremsstrahlung (see e.g. Ettori & Fabian, 2006; Markevitch, 2007; Qin & Wu, 2000). Following previous work, we define the ratio between the number densities of helium and protons

$$x = \frac{n_{\rm He}}{n_{\rm p}}. \qquad (1)$$

In the X-ray analysis, x is generally fixed to a value that will depend on the abundance table of reference. In Fig. 1 , we show the comparison between the values of x tabulated in the abundance tables available in the software adopted for our X-ray analysis (`Xspec`, Arnaud, 1996)[2] and the one from primordial nucleosynthesis, $x_{\rm BBN} = (Y_{\rm BBN}/A_{\rm He}) \sum_i A_i n_i / n_{\rm H} = 0.0869$, where we use $Y_{\rm BBN} = 0.2471$ (see previous Section) and the number densities, relative to hydrogen, tabulated in Anders & Grevesse (1989) with a metallicity of 0.3 (apart from H and He assumed to have a cosmic abundance). We note the different behaviour of two popular tables: while *angr* (Anders & Grevesse, 1989) has a value of x (0.0977) about 12% higher of x_{BBN}, *aspl* (Asplund, Grevesse, Sauval, & Scott, 2009) is well in agreement within 2% (0.0851).

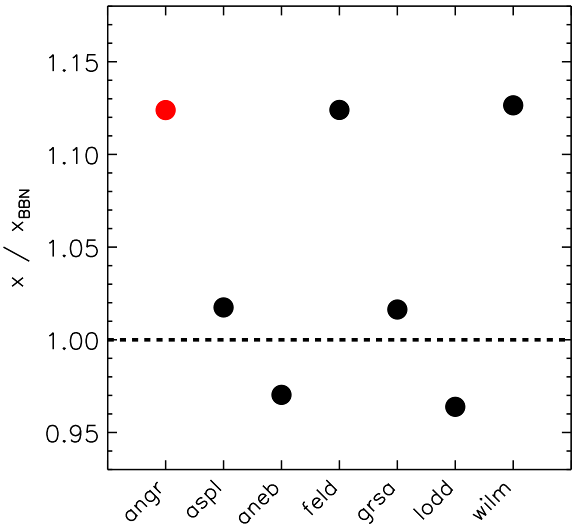

FIGURE 1 Comparison between the value of x for each of the abundance tables available in `Xspec` and listed in abscissa, and the primordial value $x_{\rm BBN}$.

The X-ray brehmsstrahlung emissivity $\epsilon = n_{\rm e} \sum (Z_i^2 n_i) \Lambda(T)$, where $n_{\rm e}$ is the electron number density and $\Lambda(T)$ is the cooling function that depends only on the gas temperature T (less significantly moving to softer energy bands in the observer rest-frame; see e.g. fig. 2 in Ettori, 2000), can be well approximated as produced mainly from nuclei of hydrogen and helium ($Z_{\rm He} = 2$): $\epsilon \propto n_{\rm e} n_{\rm p} (1+4x) \sim n_{\rm p}^2 (1+4x)(1+2x)$, where the relation $n_{\rm e}/n_{\rm p} = 1+2x$ holds. This approximation is reasonable because the contribution from other metals with atomic number $Z_i \geq 3$ raises the value of $(1+4x)(1+2x)$ by about 3%.

---

[2] see https://heasarc.gsfc.nasa.gov/xanadu/xspec/manual/node117.html

Hence, for an observed X-ray flux $f \propto \epsilon \, R^3/d_L^2$, $n_{\rm p}$ scales as $h^{0.5} \, [(1+4x)(1+2x)]^{-0.5}$, where d_L is the luminosity distance that is proportional to the Hubble constant h^{-1}, and R is the proper radius equal to the angular scale times the angular diameter distance $d_A = d_L/(1+z)^2$.

We can also write the dependence for the gas mass $M_{\rm gas}$ and the hydrostatic mass $M_{\rm hyd}$ (see e.g. Ettori et al., 2013) as

$$\begin{aligned} \mu &= \left(\sum_i \frac{X_i n_i}{A_i} \right)^{-1} \sim \frac{1+4x}{2+3x}, \\ M_{\rm gas} &\propto \mu (n_{\rm e} + n_{\rm p}) \, R^3 \sim \mu \, n_{\rm p} (2+2x) \, R^3 \\ &\sim \left(\frac{1+4x}{1+2x} \right)^{0.5} \frac{1+x}{2+3x} \, h^{-2.5}, \\ M_{\rm hyd} &\propto \mu^{-1} \, R \sim \frac{2+3x}{1+4x} \, h^{-1}, \end{aligned} \tag{2}$$

where μ is the mean molecular weight, with X_i and A_i being the mass fraction and atomic weight of element i, respectively.

In these equations, we make also evident the dependence upon the Hubble constant $h \equiv h_{70} = H_0/(70 \text{ km s}^{-1} \text{ Mpc}^{-1})$, that is propagated through the radial dependence of these quantities and that will be useful to consider in the following analysis. In general, for a fixed value of H_0, the impact of changing the helium abundance is in the order of few percent (see Fig. 2).

2.1 | Constraining x with X-ray and SZ observations of the ICM

We discuss here how using the different dependence on $x = n_{\rm He}/n_{\rm p}$ of the ICM pressure recovered, independently, from X-ray and SZ signal can constrain the helium abundance.

The X-ray pressure is the product of the spectral measurement of the gas temperature, $T_{\rm e}$, by the electron density $n_{\rm e}$ estimated by the geometrical deprojection of the observed surface brightness $S_X \propto \int n_{\rm e} n_{\rm p} (1+4x) dl$, that implies the following scaling:

$$n_{\rm e,X} \sim {\rm deproj}(S_X)^{0.5} \left(\frac{1+2x}{1+4x} \right)^{0.5} h^{0.5}. \tag{3}$$

The SZ pressure is obtained directly from the deprojection of the Compton parameter $y \propto \int n_{\rm e} T_{\rm e} \, dl$:

$$\left(n_{\rm e} T_{\rm e} \right)_{SZ} \sim {\rm deproj}(y) \, h. \tag{4}$$

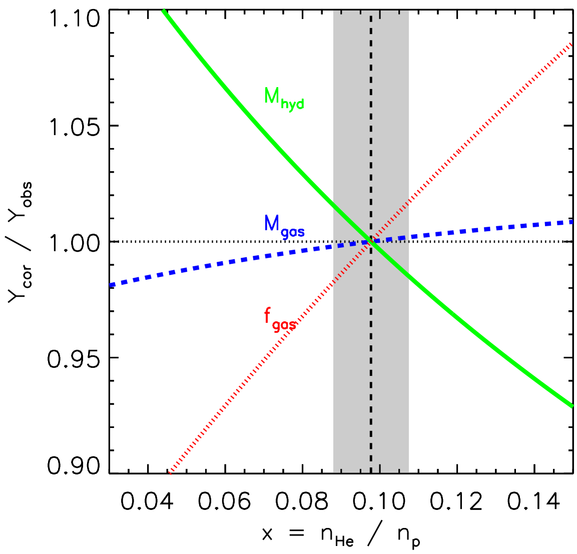

FIGURE 2 Variations with x of $M_{\rm gas}$ (blue dashed line), $M_{\rm hyd}$ (green solid line) and $f_{\rm gas} = M_{\rm gas}/M_{\rm hyd}$ (red dotted line) for a fixed value of H_0. The vertical line indicates the helium abundance from *angr*, $x = 0.0977$, with ±10% represented by the shaded area.

In both cases, dl indicates that the integration occurs along the light of sight and is thus proportional to the angular diameter distance and, hence, to h^{-1}.

Under the assumption of spherical symmetry, and that the gas density reconstructed from X-ray is not affected from clumpiness (e.g. Nagai & Lau, 2011; Roncarelli et al., 2013) that might bias high its value, we can write the ratio between the two estimates of the pressure as

$$\frac{P_{SZ}}{P_X} = \frac{\left(n_{\rm e} T_{\rm e} \right)_{SZ}}{n_{\rm e,X} T_{\rm e}} \sim \left(\frac{1+4x}{1+2x} \right)^{0.5} h^{0.5} = \eta. \tag{5}$$

The quantity $\eta = \theta^{0.5} \, h^{0.5}$, where $\theta = (1+4x)/(1+2x)$, is then the one that we want to measure to constrain x (as originally suggested by Markevitch, 2007), also relying on independent measurements of the Hubble constant. In the present work, we adopt the following values (with relative uncertainties) for the Hubble constant: $H_{0,CMB} = 67.4 \pm 0.5$ km s^{-1} Mpc^{-1} from the *Planck* measurements of the CMB anisotropies, combining information from the temperature and polarization maps and the lensing reconstruction, assuming a spatially-flat 6-parameter ΛCDM cosmology (Planck Collaboration et al., 2018); $H_{0,LMC} = 74.03 \pm 1.42$ km s^{-1} Mpc^{-1} from Hubble Space Telescope observations of 70 long-period Cepheids in the Large Magellanic Cloud, combined with masers in NGC 4258, and Milky Way parallaxes (Riess, Casertano, Yuan, Macri, & Scolnic, 2019). These values embrace the actual extremes of the distribution of H_0. For example, other recent constraints are the one based on the tip of the Red

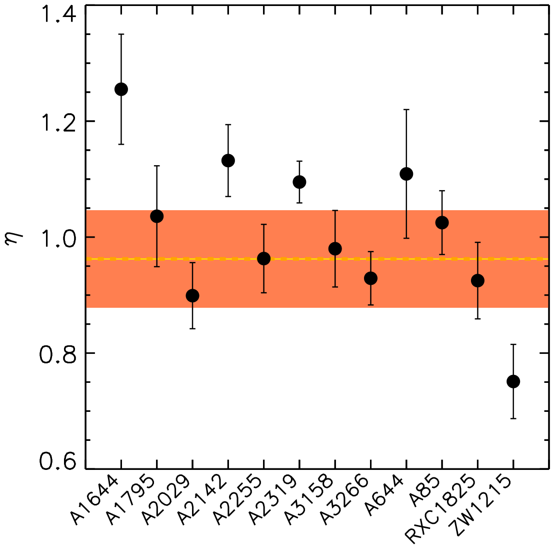

FIGURE 3 Result on the parameter $\eta = P_{SZ}/P_X$ obtained from a best-fit of the pressure profiles for each X-COP object. The coloured areas indicate the scatter (0.0838) in the distribution and the error (0.0013) on the central position of the joint-fit value $\eta_{X-COP} = 0.9624$, used in the present analysis. See also appendix in Ghirardini et al. (2019).

Giant Branch (Freedman et al., 2019), that provides a value of $H_{0,TRGB} = 69.8$ km s^{-1} Mpc^{-1}, and a measurement of $H_{0,delay} = 73.3$ km s^{-1} Mpc^{-1} that relies on the joint analysis of six gravitationally lensed quasars with measured time delays (Wong et al., 2019), both with a relative uncertainty of ~ 2.4–2.6 % (see further discussion in Verde, Treu, & Riess, 2019).

It is worth noticing that, reversely, by assuming known x, the method can be used to constrain H_0 (e.g. Cavaliere, Danese, & de Zotti, 1979; Silk & White, 1978) as discussed recently in an extensive way by Kozmanyan, Bourdin, Mazzotta, Rasia, & Sereno (2019).

3 | CONSTRAINTS ON X

In this section, we present the sample of galaxy clusters that we have analyzed to recover both P_X and P_{SZ}, and to constrain η and hence $x = n_{\rm He}/n_{\rm p}$.

3.1 | The X-COP sample

The *XMM-Newton* Cluster Outskirts Project (X-COP[3], Eckert et al., 2017) is an *XMM* Very Large Program dedicated to the study of the X-ray emission in cluster outskirts. It has targeted 12 local, massive galaxy clusters selected for their high signal-to-noise ratios in the *Planck* all-sky SZ survey (S/N> 12 in the PSZ1 sample, Planck Collaboration et al., 2014) as resolved sources ($R_{500} > 10$ arcmin) in the redshift range $0.04 < z < 0.1$ and along the directions with a galactic absorption lower than 10^{21} cm^{-2} to avoid any significant suppression of the X-ray emission in the soft band where most of the spatial analysis is performed. These selection criteria guarantee that a joint analysis of the X-ray and SZ signals allows the reconstruction of the ICM properties out to $R_{200} (\approx 1.5 R_{500})$ for all our targets. A complete description of the reduction and analysis of our proprietary X-ray data and of the *Planck* SZ data is provided in Ghirardini et al. (2019) (see also Eckert et al., 2019; Ettori et al., 2019). Here, we want only to remark that a proper treatment of the X-ray surface brightness profiles, accounting for the median of the distribution of the counts per pixel in a given radial annulus instead of the mean (e.g. Eckert et al., 2015; Zhuravleva et al., 2013), guarantees in the X-COP analysis against a relevant contribution from clumped gas that might systematically bias the estimate of the gas density (Eq. 3).

Finally, we have to initialize our measurement of η, by considering the conversion factors applied in our X-ray analysis, that is the only part in the calculation of η where x appears (see Eq. 3 and 4). As detailed in Ghirardini et al. (2019), we consider a 30% solar abundance metallicity, as in Anders & Grevesse (1989), to convert the emissivity $n_{\rm e} \sum (Z_i^2 n_i)$ to 1.7181 $n_{\rm p}^2$, and a fixed relation $n_{\rm e} = 1.17 n_{\rm p}$, implying that $\eta = \eta_{X-COP} \left(1.7181/1.17^2\right)^{0.5}$, where $\eta_{X-COP} = 0.9624 \pm 0.0013$ (r.m.s. 0.0838; see Fig. 3) is the joint best-fit of the SZ and X-ray pressure profiles recovered for the X-COP sample. This joint fit mitigates any bias in the assumed spherical symmetry, in particular, of the SZ signal, where it is assumed that the line-of-sight gas distribution is the same as that in the plane of the sky. In the following analysis, we consider the error on the central value as statistical uncertainty of η, whereas the dispersion around it indicates the limitations still present in our modelization of η (see Sect. 4).

3.2 | $\eta + H_0$: results on x

From the measurements of η obtained in the X-COP sample and the adopted values of H_0 (see subsection 2.1), we can use Equation 5 to estimate $\theta = \eta^2/h$. We show the constraints on θ in Fig. 4 . Low values of x, lower than the one (*angr*) adopted in the X-COP X-ray analysis seem to be preferred from high values of the Hubble constant. In particular, for $H_{0,LMC}$ (74 km s^{-1} Mpc^{-1}), $x = 0.055 \pm 0.013$, whereas for $H_{0,CMB}$ (67.4 km s^{-1} Mpc^{-1}), $x = 0.131 \pm 0.008$. These values should be compared with a cosmic value of $x_{BBN} = 0.0869$ and $x = 0.0977$ for the abundance table in *angr*.

---

[3] `https://www.astro.unige.ch/xcop`

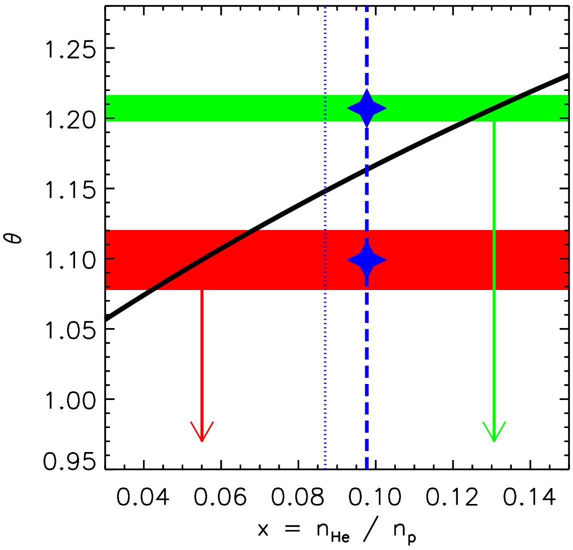

FIGURE 4 Constraints on $\theta = \eta^2/h$, and relative uncertainties at 1σ, assuming $H_{0,CMB}$ (green area) and $H_{0,LMC}$ (red area). The blue stars indicate the central value for the adopted value of x in the X-COP X-ray analysis (*angr*: dashed line; cosmological value: dotted line). The black solid line represents $\theta = (1+4x)/(1+2x)$. The coloured arrows indicate the preferred values of x for a given θ. High values of H_0 tend to prefer low values of x.

Reversely, fixing x equal to the values from BBN, *aspl*, *angr*, we measure $H_0 = 70.9, 71.0, 69.9$ km s^{-1} Mpc^{-1}, respectively, with a statistical error of 0.2 (12, when the scatter is considered) km s^{-1} Mpc^{-1}.

3.3 | Corrections on the derived quantities

From Fig. 4 , we can derive, for each assumed value of H_0, the expected $\bar{\theta}$ and, then, the corresponding $\bar{x}$. Thus, we can associate to a given H_0 the correction which propagates to the gas mass and to the hydrostatic mass through x, accordingly to the scaling presented in Eq. 2 and accounting for the dependence both on x and on H_0. We show in Fig. 5 the total correction on these quantities. Overall, the corrections should be less than ~ 15%, with lower tension (below 10%) obtained with $H_{0,CMB}$. Note that the estimated difference with respect to the reconstructed value of $M_{\rm hyd}$ is, in both cases, of few per cent and well below the hydrostatic bias measured by using weak lensing mass estimates.

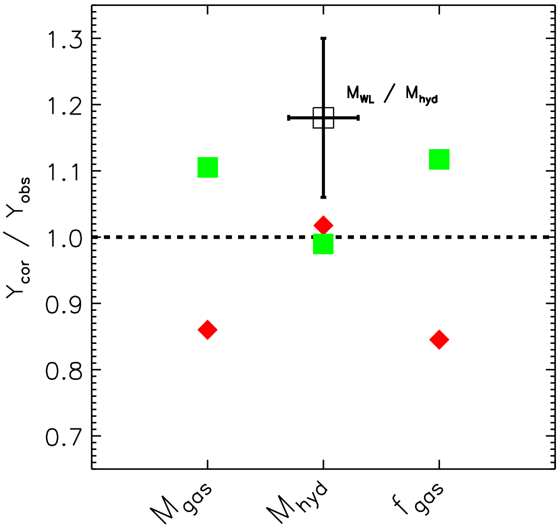

FIGURE 5 Total corrections on $M_{\rm gas}$, $M_{\rm hyd}$ and $f_{\rm gas}$, assuming $H_{0,CMB}$ (green squares) and $H_{0,LMC}$ (red diamonds). The correction on the hydrostatic mass is compared with the measured tension with weak-lensing estimates for a subsample of 6 X-COP objects (for details, see Ettori et al., 2019).

We present also the correction propagated to the gas mass fraction $f_{\rm gas} = M_{\rm gas}/M_{\rm hyd}$ through the scaling presented in Eq. 2. We can write this correction in a way similar to the form adopted to represent how the fraction α_P of the non-thermal pressure with respect to the total one (and equivalent to the hydrostatic bias b, when α_P does not vary with the radius) propagates into the estimate of $f_{\rm gas}$ (see e.g. Eq. 8 in Eckert et al., 2019):

$$\frac{f_{\rm gas,true}}{f_{\rm gas,obs}} = \frac{f_{\rm gas,true}}{f_{\rm gas,cor}} \frac{f_{\rm gas,cor}}{f_{\rm gas,obs}} = (1-\alpha_P)(1-\alpha_c), \qquad (6)$$

where $f_{\rm gas,obs}$ is the observed gas fraction, $f_{\rm gas,true}$ is the expected "true" gas fraction, and $f_{\rm gas,cor}$ is the gas fraction after the correction by its dependence on the quantity x and the Hubble constant h (from $M_{\rm gas}$ and $M_{\rm hyd}$ in Eq. 2). In Fig. 6 , we show the constraints we obtain on α_c. Once again, the expected (either cosmological or from the adopted solar abundance) helium density lies between the amount required from the considered H_0, with values of x below the canonical range of 0.08–0.1 corresponding to H_0 above 70 km s^{-1} Mpc^{-1}.

4 | CONCLUSIONS

We have discussed the role of the helium abundance on the observed properties of the ICM in a well-selected sample of nearby massive galaxy clusters with independent X-ray and SZ measurements.

We obtain that the present constraints on the Hubble constant require central values of $x = n_{\rm He}/n_{\rm p}$ between 0.055

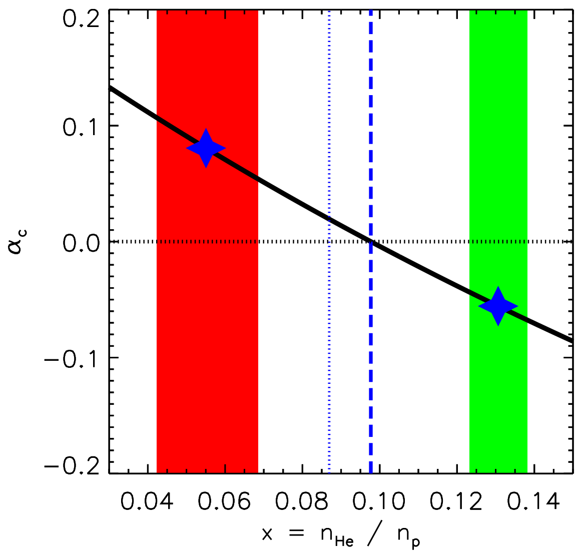

FIGURE 6 Constraints on α_c (see Eq. 6). As in Fig. 4 , the assumed H_0 is colour-coded (green: $H_{0,CMB}$; red: $H_{0,LMC}$). The blue stars indicate the central value for x, to be compared with the value adopted in the X-ray analysis (*angr*, dashed line) and the cosmological value (dotted line).

(for $H_{0,LMC}$ = 74 km s^{-1} Mpc^{-1}) and 0.131 (for $H_{0,CMB}$ = 67.4 km s^{-1} Mpc^{-1}), that encompass the assumed value in the X-ray analysis ($x = 0.0977$ for the abundance table in Anders & Grevesse, 1989) and the cosmological one inferred from BBN ($x_{\rm BBN} = 0.0869$). In any case, values of H_0 around 70 km s^{-1} Mpc^{-1} are preferred from our estimates of $\eta = P_{SZ}/P_X = \theta^{0.5} h^{0.5}$, with $\theta = (1+4x)/(1+2x)$, if x has to lie around values of 0.08–0.1. While higher values of x, requiring lower estimates of H_0, can be partially explained with an efficient process of sedimentation, a reduction of the helium abundance (implying $H_0 > 70$ km s^{-1} Mpc^{-1}) can be obtained by the action of thermal diffusion (e.g. Medvedev, Gilfanov, Sazonov, & Shtykovskiy, 2014). On the other hand, magnetic fields and mixing effects of large-scale turbulence are known to play a role in shaping the ICM properties, also by reducing significantly the impact of the above mentioned processes. On the contrary, fixing x to the values from BBN, Asplund et al. (2009) and Anders & Grevesse (1989), we obtain $H_0 = 70.9, 71.0, 69.9$ (1 σ error: 0.2; 12, when the scatter in the distribution of η -see Fig. 3 - is propagated) km s^{-1} Mpc^{-1}, respectively.

A further improvement both on the statistical and systematic uncertainty of the estimate of η will be obtained with larger samples of X-ray and SZ estimates of the ICM pressure with respect to the dataset of 12 values from the X-COP sample. One of these samples will be obtained by our dedicated *XMM-Newton* Heritage program [4], that will enlarge by a factor of ∼10 the number of measurements of η, allowing to reduce by $\sqrt{10} \sim 3.2$ the statistical error and to lower more significantly the impact of the assumed spherical geometry of the ICM distribution.

ACKNOWLEDGMENTS

The research leading to these results has received funding from the European Union's Horizon 2020 Programme under the AHEAD project (grant agreement n. 654215). S.E. acknowledges financial contribution from the contracts ASI 2015-046-R.0 and ASI-INAF n.2017-14-H.0.

REFERENCES

Anders, E., & Grevesse, N. 1989, January, *Geochim. Cosmochim. Acta*, *53*, 197-214. doi:
Arnaud, K. A. 1996, XSPEC: The First Ten Years. G. H. Jacoby & J. Barnes (Eds.), Astronomical Data Analysis Software and Systems V Vol. 101, p. 17.
Asplund, M., Grevesse, N., Sauval, A. J., & Scott, P. 2009, Sep, *ARA&A*, *47*(1), 481-522. doi:
Aver, E., Olive, K. A., & Skillman, E. D. 2015, Jul, *J. Cosmology Astropart. Phys.*, *2015*(7), 011. doi:
Bulbul, G. E., Hasler, N., Bonamente, M., Joy, M., Marrone, D., Miller, A., & Mroczkowski, T. 2011, Sep, *A&A*, *533*, A6. doi:
Cavaliere, A., Danese, L., & de Zotti, G. 1979, Jun, *A&A*, *75*(3), 322-325.
Eckert, D., Ettori, S., Pointecouteau, E., Molendi, S., Paltani, S., & Tchernin, C. 2017, March, *Astronomische Nachrichten*, *338*, 293-298. doi:
Eckert, D., Ghirardini, V., Ettori, S. et al. 2019, Jan, *A&A*, *621*, A40. doi:
Eckert, D., Roncarelli, M., Ettori, S., Molendi, S., Vazza, F., Gastaldello, F., & Rossetti, M. 2015, March, *MNRAS*, *447*, 2198-2208. doi:
Ettori, S. 2000, Jan, *MNRAS*, *311*(2), 313-316. doi:
Ettori, S., Donnarumma, A., Pointecouteau, E., Reiprich, T. H., Giodini, S., Lovisari, L., & Schmidt, R. W. 2013, August, *Space Sci. Rev.*, *177*, 119-154. doi:
Ettori, S., & Fabian, A. C. 2006, Jun, *MNRAS*, *369*(1), L42-L46. doi:
Ettori, S., Ghirardini, V., Eckert, D. et al. 2019, Jan, *A&A*, *621*, A39. doi:
Freedman, W. L., Madore, B. F., Hatt, D. et al. 2019, Jul, *arXiv e-prints*, arXiv:1907.05922.
Ghirardini, V., Eckert, D., Ettori, S. et al. 2019, Jan, *A&A*, *621*, A41. doi:
Hitomi Collaboration, Aharonian, F., Akamatsu, H. et al. 2018a, Mar, *PASJ*, *70*(2), 9. doi:
Hitomi Collaboration, Aharonian, F., Akamatsu, H. et al. 2018b, Mar, *PASJ*, *70*(2), 12. doi:

---

[4] `http://xmm-heritage.oas.inaf.it/`

Kozmanyan, A., Bourdin, H., Mazzotta, P., Rasia, E., & Sereno, M. 2019, Jan, *A&A*, *621*, A34. doi:

Markevitch, M. 2007, May, *arXiv e-prints*, arXiv:0705.3289.

Medvedev, P., Gilfanov, M., Sazonov, S., & Shtykovskiy, P. 2014, May, *MNRAS*, *440*(3), 2464-2473. doi:

Nagai, D., & Lau, E. T. 2011, April, *ApJ*, *731*, L10. doi:

Pitrou, C., Coc, A., Uzan, J.-P., & Vangioni, E. 2018, Sep, *Phys. Rep.*, *754*, 1-66. doi:

Planck Collaboration, Ade, P. A. R., Aghanim, N. et al. 2014, November, *A&A*, *571*, A29. doi:

Planck Collaboration, Aghanim, N., Akrami, Y. et al. 2018, Jul, *arXiv e-prints*, arXiv:1807.06209.

Qin, B., & Wu, X.-P. 2000, Jan, *ApJ*, *529*(1), L1-L4. doi:

Riess, A. G., Casertano, S., Yuan, W., Macri, L. M., & Scolnic, D. 2019, May, *ApJ*, *876*(1), 85. doi:

Roncarelli, M., Ettori, S., Borgani, S., Dolag, K., Fabjan, D., & Moscardini, L. 2013, July, *MNRAS*, *432*, 3030-3046. doi:

Sanders, J. S., & Fabian, A. C. 2013, Mar, *MNRAS*, *429*(3), 2727-2738. doi:

Silk, J. 1968, Feb, *ApJ*, *151*, 459. doi:

Silk, J., & White, S. D. M. 1978, Dec, *ApJ*, *226*, L103-L106. doi:

Spitzer, L. 1956, Physics of Fully Ionized Gases. New York: Interscience Publishers.

Sunyaev, R. A., & Zeldovich, Y. B. 1972, November, *Comments on Astrophysics and Space Physics*, *4*, 173.

Verde, L., Treu, T., & Riess, A. G. 2019, Jul, *arXiv e-prints*, arXiv:1907.10625.

Wong, K. C., Suyu, S. H., Chen, G. C. F. et al. 2019, Jul, *arXiv e-prints*, arXiv:1907.04869.

Zhuravleva, I., Churazov, E., Kravtsov, A., Lau, E. T., Nagai, D., & Sunyaev, R. 2013, February, *MNRAS*, *428*, 3274-3287. doi: